

Fractal zone plates with variable lacunarity

Juan A. Monsoriu

Departamento de Física Aplicada, Universidad Politécnica de Valencia, E-46022 Valencia, Spain

Genaro Saavedra, and Walter D. Furlan

Departamento de Óptica, Universitat de València, E-46100 Burjassot, Spain
walter.furlan@uv.es

Abstract: Fractal zone plates (FZPs), i.e., zone plates with fractal structure, have been recently introduced in optics. These zone plates are distinguished by the fractal focusing structure they provide along the optical axis. In this paper we study the effects on this axial response of an important descriptor of fractals: the lacunarity. It is shown that this parameter drastically affects the profile of the irradiance response along the optical axis. In spite of this fact, the axial behavior always has the self-similarity characteristics of the FZP itself.

©2004 Optical Society of America

OCIS codes: (050.1940) diffraction; (050.1970) diffractive optics;

References and links

1. J. Ojeda-Castañeda and C. Gómez-Reino, Eds., *Selected papers on zone plates* (SPIE Optical Engineering Press, Washington, 1996).
2. S. Wang, X. Zhang, "Terahertz tomographic imaging with a Fresnel lens," *Opt. Photon. News* **13**, 59 (2002).
3. Y. Wang, W. Yun, and C. Jacobsen, "Achromatic Fresnel optics for wideband extreme-ultraviolet and X-ray imaging," *Nature* **424**, 50-53 (2003).
4. L. Kipp, M. Skibowski, R. L. Johnson, R. Berndt, R. Adelung, S. Harm, and R. Seemann, "Sharper images by focusing soft x-rays with photon sieves," *Nature* **414**, 184-188 (2001).
5. Q. Cao and J. Jahns, "Modified Fresnel zone plates that produce sharp Gaussian focal spots," *J. Opt. Soc. Am. A* **20**, 1576-1581 (2003).
6. Q. Cao and J. Jahns, "Comprehensive focusing analysis of various Fresnel zone plates," *J. Opt. Soc. Am. A* **21**, 561-571 (2004).
7. G. Saavedra, W.D. Furlan, and J.A. Monsoriu, "Fractal zone plates," *Opt. Lett.* **28**, 971-973 (2003).
8. W.D. Furlan, G. Saavedra, and J.A. Monsoriu, "Fractal zone plates produce axial irradiance with fractal profile," *Opt. & Photon. News* **28**, 971-973 (2003).
9. J.A. Davis, L. Ramirez, J.A. Rodrigo Martín-Romo, T. Alieva, and M.L. Calvo, "Focusing properties of fractal zone plates: experimental implementation with a liquid-crystal display," *Opt. Lett.* **29**, 1321-1323 (2004).
10. B. Mandelbrot, *The Fractal Geometry of Nature* (Freeman, San Francisco, 1982).
11. A.D. Jaggard and D.L. Jaggard, "Cantor ring diffractals," *Opt. Commun.* **158**, 141-148 (1998).
12. L. Zunino and M. Garavaglia, "Fraunhofer diffraction by Cantor fractals with variable lacunarity," *J. Mod. Opt.* **50**, 717-727 (2003).
13. Y. Sakurada, J. Uozumi, and T. Asakura, "Fresnel diffraction by 1-D regular fractals," *Pure Appl. Opt.* **1**, 29-40 (1992).
14. H. Melville and G. F. Milne, "Optical trapping of three-dimensional structures using dynamic holograms," *Opt. Express* **11**, 3562-3567 (2003).

1. Introduction

A renewed interest in zone plates [1] has been experienced during the last years because they are becoming key elements used to obtain images in several scientific and technological areas such as, THz tomography and soft X-ray microscopy [2-6]. With this motivation, we have recently proposed the fractal zone plates (FZPs) as new promising 2D photonic structures [7,8]. Lately, FZPs were implemented experimentally with a liquid crystal display by Davis et

al. [9]. A FZP can be thought as a conventional zone plate with certain missing zones. The resulting structure is characterized by its fractal profile along the square of the radial coordinate. The axial irradiance provided by a FZP when illuminated with a parallel wavefront presents multiple foci, the main lobe of which coincide with those of the associated conventional zone plate. However, the internal structure of each focus exhibits a characteristic fractal structure, reproducing the self-similarity of the originating FZP. In this way, synthesis of axial irradiances with fractal profile can be achieved easily given the simple theoretical relation between the transmittance of the FZP and their axial response [7].

In this paper, we analyze the axial response of FZPs to a specific design parameter, frequently used as a measure of the “texture” of fractal structures: the lacunarity. In particular, we focus our attention on binary amplitude Cantor-like FZPs. First, some practical considerations about the design of this type of FZPs are investigated, taking into account the physical limits imposed by the different construction parameters. Finally, the axial irradiance provided by FZPs with variable lacunarity is numerically evaluated, and compared with the response of regular FZPs.

2. Theory

Let us consider the irradiance at a given point on the optical axis, provided by a rotationally invariant pupil with an amplitude transmittance $p(r)$, illuminated by a monochromatic plane wave. Within the Fresnel approximation, this magnitude is given as a function of the axial distance from the pupil plane R , as

$$I(R) = \left(\frac{2\pi}{\lambda R} \right)^2 \left| \int_0^a p(r_o) \exp\left(-i \frac{\pi}{\lambda R} r_o^2\right) r_o \, dr_o \right|^2. \quad (1)$$

In Eq. (1), a is the maximum extent of the pupil function $p(r)$ and λ is the wavelength of the light. For our purposes it is convenient to express the pupil transmittance as function of a new variable defined as

$$\zeta = \left(\frac{r_o}{a} \right)^2 - 0.5, \quad (2)$$

in such a way that $q(\zeta) = p(r_o)$. By using the dimensionless reduced axial coordinate $u = a^2/2\lambda R$, the irradiance along the optical axis can be expressed simply in terms of the Fourier transform of $q(\zeta)$ as

$$I_o(u) = 4\pi^2 u^2 \left| \int_{-0.5}^{+0.5} q(\zeta) \exp(-i 2\pi u \zeta) \, d\zeta \right|^2. \quad (3)$$

Note that the reduced axial coordinate can also be expressed in terms of the Fresnel number F as $u = F/2$.

Now, if the pupil function $q(\zeta)$ holds a fractal structure, it is well known that the Fourier transform preserves fractal properties [10], and then, it is direct to conclude that such pupil will provide irradiance along the optical axis also with a fractal profile.

The comparison between a conventional zone plate and a FZP can be done taking into account the change of variables in Eq. (2). For a conventional zone plate the function $q(\zeta)$ is a periodic function. In a similar way, a FZP results if $q(\zeta)$ represents any self-similar (fractal) 1-D function. In particular we will focus our attention in functions $q(\zeta)$ constructed from different levels of a polyadic Cantor set.

3. Cantor-like FZP design

The construction of a typical polyadic Cantor fractal set is shown in Fig. 1. The first step consists in defining a straight-line segment of unit length called *initiator* (stage $S=0$). Next, at stage $S=1$, the *generator* of the set is constructed by N ($N=4$ in the figure) non-overlapping copies of the initiator, each one with a scale $\gamma < 1$, distributed in a particular way into the unit length segment. At the following stages of the construction of the set ($S=2,3,\dots$), the generation process is repeated over and over again for each segment in the previous stage. To characterize the resulting Cantor set, as well as many other fractal structures, one of the most frequently used descriptors is the *fractal dimension*, defined as

$$D = -\ln(N)/\ln(\gamma). \quad (4)$$

However, the fractal dimension does not uniquely define the fractal. In fact, for the most general case, it is necessary to introduce another parameter to specify the distribution of the N copies into the unit length segment at $S=1$. In other words, a parameter to specify the lacunarity (or “gapinness”) of the resulting structure is needed. In this work, as in previous papers dealing with Cantor fractals in optics [11,12], we used the width of outermost gap in the first stage, ε (see Fig. 1) for this purpose.

The construction parameters of a FZP are linked to each other, and also they must satisfy certain constraints. On the one hand, the maximum value of the scale, γ_{max} , depends on the value of N , i.e., $0 \leq \gamma_{max} \leq N^{-1}$. On the other hand, for each value of N and γ , there are two extreme values for ε . For the first, $\varepsilon=0$, the result is the highest lacunar fractal, having the central gap very large while the outer ones become null. The other extreme value of ε is

$$\varepsilon_{max} = \frac{1 - N\gamma}{N - 2}. \quad (5)$$

In this case, a lower lacunar structure than in the previous case is obtained, since the central gap is missed. A particular value of ε that gives the lowest lacunar (or *regular*) fractal exists between *zero* and ε_{max} . This value of ε , which is obtained by imposing bars and gaps to have the same size at the initiator stage (as done in Ref. [7]), is given by

$$\varepsilon_R = \frac{1 - N\gamma}{N - 1}. \quad (6)$$

The influence of these construction parameters is shown in Fig. 2. FZPs are generated from Cantor bars like the one in the middle row of Fig. 1, i.e., $N=4$ and $S=1$, first by use of Eq. (2), and then by rotating the re-scaled bars around one of the extremes. FZPs for three different values of γ are obtained. The animations in this figure show the evolution of the FZP for values of ε ranging from zero to ε_{max} . According to our previous discussion, it can be seen that by changing ε , different structures with the same fractal dimension can be obtained.

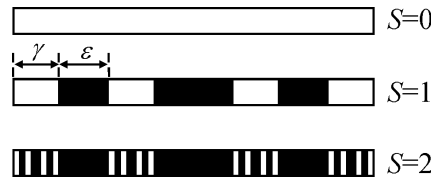


Fig. 1. Schemes for the generation of the FZP binary function $q(\zeta)$ for $N=4$ up to $S=2$. γ is the scale factor and ε is the parameter that characterizes the lacunarity.

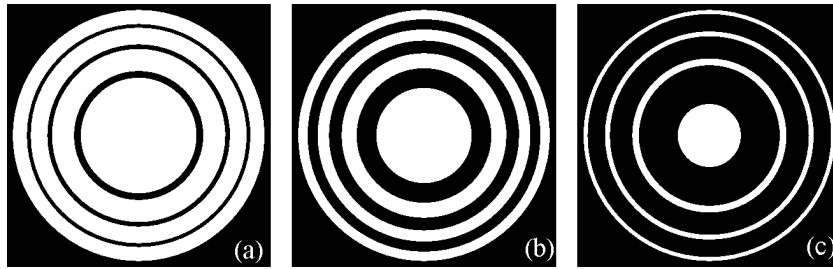


Fig. 2. FZPs generated with the following parameters: (a) $\gamma=4/19$, $\varepsilon=1/19$; (b) $\gamma=1/7$, $\varepsilon=1/7$; and (c) $\gamma=1/16$, $\varepsilon=1/4$. In all cases: $N=4$, $S=1$ and $\varepsilon = \varepsilon_R$. The animations fig2a.gif (332kB), Fig. 2(b).gif (341kB) and Fig. 2(c).gif (323kB) show the evolution of the resulting FZPs for a variable lacunarity, ε varying from zero to ε_{max} . Note that ε_{max} is different in each case (see Eq. (5)), being: a) 3/38; b) 3/14; and c) 3/8.

Summarizing, the number of stages, the lacunarity, the fractal dimension and the scale, are the independent variables in the construction of a FZP. Their influence on the axial irradiance will be presented in the next section.

4. Fractal behavior of the axial irradiance

Interesting features about the axial irradiance provided by regular FZPs were previously reported in Ref. [7]. In particular, we called *axial scale property* to the fact (theoretically supported by Eq. (3) that the axial irradiance reproduces the self-similarity of the FZP. In this section we will analyze the influence of the lacunarity on this property.

Since for the regular case the axial irradiance is a periodic function of the coordinate u with period $u_p=1/\gamma^S$ [7], one way to observe the axial fractal behavior of the irradiance is by representing it as a function of the reduced axial coordinate as $u/u_p = \gamma^S u$. Figure 3(a) shows the FZP constructed with the same parameters as in Fig. 2(b), but for $S=2$. The normalized axial irradiances given by these two pupils ($S=1$ and $S=2$) for $\varepsilon=\varepsilon_R$ are represented with different colors in Fig. 3(b). The self-similarity between these patterns can be clearly seen: the blue pattern is a magnified version of the red one, and the later is an envelope of the former. The animation in this figure shows the change the FZPs experiences for different values of the lacunarity (ε ranging from $\varepsilon=0$ to ε_{max}), and at the same time, the evolution of the axial irradiance provided by this pupils. It can be seen that the optical irradiance produced by the FZPs is highly influenced by the lacunarity.

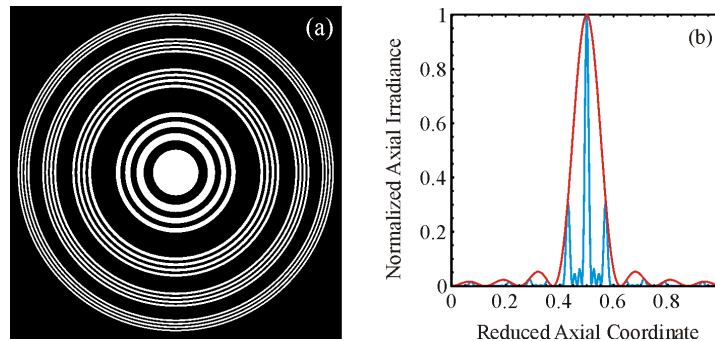


Fig. 3. (a) FZP generated with the following parameters: $\gamma=1/7$, $\varepsilon=\varepsilon_R=1/7$, $N=4$, and $S=2$ (compare it with Fig. 2b). (b) Normalized axial irradiances obtained with the FZP in a) and with the FZP in Fig. 2b). The animation Fig. 3.gif (905kB) shows the evolution of the FZP for a variable lacunarity, ε varying from zero to ε_{max} , and the corresponding axial irradiances for the above mentioned FZPs.

Nevertheless, it is clear that in all cases the irradiance for $S=2$ is still modulated by the irradiance for $S=1$. Although it seems that the self-similarity observed for the regular FZP ($\varepsilon=\varepsilon_R$) is not supported by other values of ε , this effect is an artifact due to the axial scale used in this figure. Another interesting result which is masked in Fig. 3 by the use of the normalized axial coordinate is the fact that there exists certain axial positions with zero axial irradiance for all values of ε . These effects can be better seen in Fig.4 .

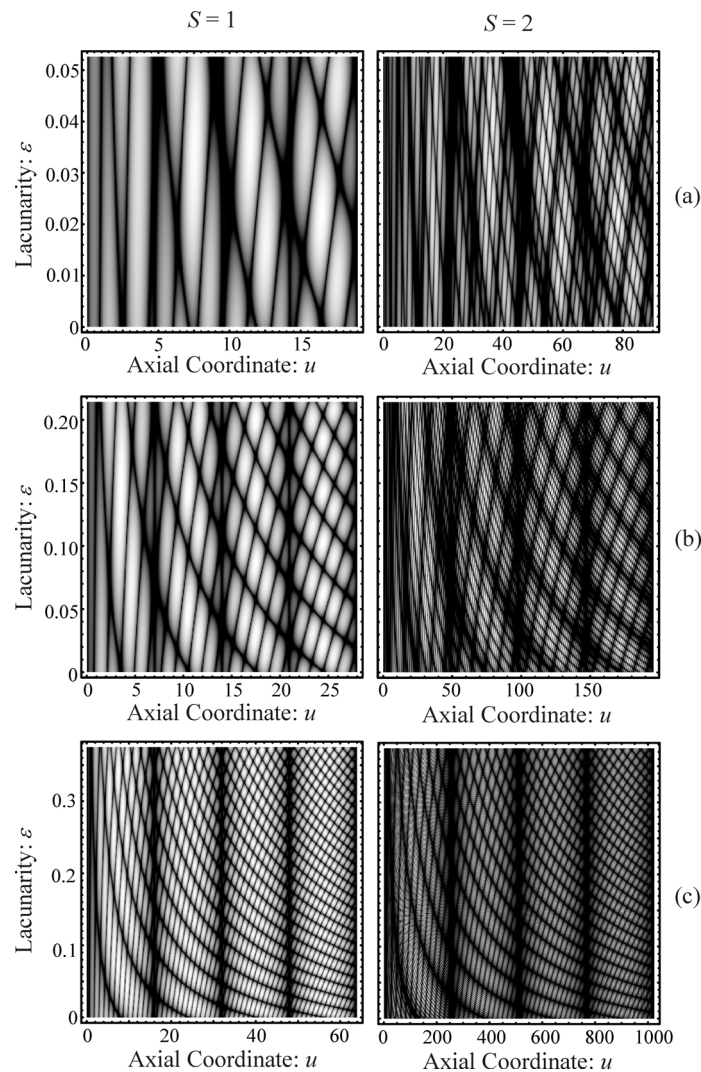


Fig. 4. Gray-scale representation of the axial irradiance (in dB) plotted as a function of the normalized axial coordinate and the lacunarity (*twist plots*). Left and right correspond to the pupils shown in Fig. 2 and the corresponding ones with $S=2$, respectively.

In this figure the axial coordinate is extended to cover several periods of the regular case. The normalized axial irradiances (as a function of u) are represented as gray levels for six families of FZPs: the three of Fig. 2 corresponding to $S=1$ (left) and other three with the same parameters but for $S=2$ (right). These irradiances were computed for the whole range of ε and then stacked sequentially to obtain these 2D displays (coined as *twist plots* [11]). The first

common aspect to be noted in all pictures are the vertical dark bands corresponding to axial nulls whose positions remain invariant with the lacunarity. These nulls are obtained at values $u = i/\gamma^S$ (for $i=1, 2, \dots$), and are caused by the destructive axial interference between all points inside each individual ring with the same scale factor γ . In a similar way, the other nulls in this figure can be understood as multiple cross-interferences between different rings of the FZP. Fig. 4 also shows that the re-scaled data in the stage $S=1$ forms an envelope for the data at the $S=2$ and both structures are self-similar for any value of ε . This result shows that FZPs have self-similar properties similar to those reported for other Cantor-related structures [11,12].

To analyze how the axial irradiance changes with the lacunarity we used a generalization of the correlation coefficient defined by Sakurada *et al.* [13] for measuring the self-similarity. In our case the axial irradiances for a variable lacunarity were correlated with the same function computed for $\varepsilon=\varepsilon_R$, since this particular value of ε gives the lowest lacunar FZP. Thus, the correlation coefficient we used is given by

$$C(\varepsilon) = \frac{\int_0^{\infty} I_{\varepsilon_R}(u) \cdot I_{\varepsilon}(u) du}{\sqrt{\int_0^{\infty} I_{\varepsilon_R}^2(u) du \int_0^{\infty} I_{\varepsilon}^2(u) du}}. \quad (7)$$

From its definition, the function $C(\varepsilon)$ is expected to be a continuous function, having an absolute maximum value at $\varepsilon=\varepsilon_R$. Since the infinite limits in the integrations in Eq. (7) would pose difficulties to the accurate numerical evaluation of $C(\varepsilon)$, a more suitable expression can be obtained by using Eq. (3) and the Rayleigh's theorem. In this way, $C(\varepsilon)$ can be written as

$$C(\varepsilon) = \frac{\int_{-1}^1 [q_{\varepsilon_R}(\zeta) \otimes q_{\varepsilon_R}(\zeta)] \cdot [q_{\varepsilon}(\zeta) \otimes q_{\varepsilon}(\zeta)] d\zeta}{\sqrt{\int_{-1}^1 [q_{\varepsilon_R}(\zeta) \otimes q_{\varepsilon_R}(\zeta)]^2 d\zeta \int_{-1}^1 [q_{\varepsilon}(\zeta) \otimes q_{\varepsilon}(\zeta)]^2 d\zeta}}. \quad (8)$$

With this definition the integrals in Eq. (8) are compact supported and the degree of similarity between axial irradiances can be more precisely numerically evaluated. Moreover, this definition is instructive to see how the changes in the FZP produced by the lacunarity are correlated with the axial responses. In Fig. 5 we have represented the autocorrelations in Eq. (8) for the FZPs of Fig. 2. The black and red lines represent the correlation for the regular case, and for $\varepsilon=\varepsilon_{max}$, respectively. The graphs in the right column show the variation of the correlation coefficient for the whole range of ε . As can be seen the maximum value is attained for $\varepsilon=\varepsilon_R$. Note the different scale in the three figures, due to the range of available values of ε . The animations in this figure show the evolution of the correlation coefficient as a function of ε and at the same time the value of the autocorrelations of the product in Eq. (8). The function $C(\varepsilon)$ was also computed for different values of S . The result is shown in Fig. 6. Compared with the result obtained for $S=1$ in Fig. 5, the correlation coefficient for $S=2$ present a higher number of maxima and minima and seems to be a modulated version of the previous stage. Interestingly, it seems that, to a certain extent, the function $C(\varepsilon)$ has also a fractal behavior, though limited for the range of ε available for each value of γ . This last result is a new property of FZPs.

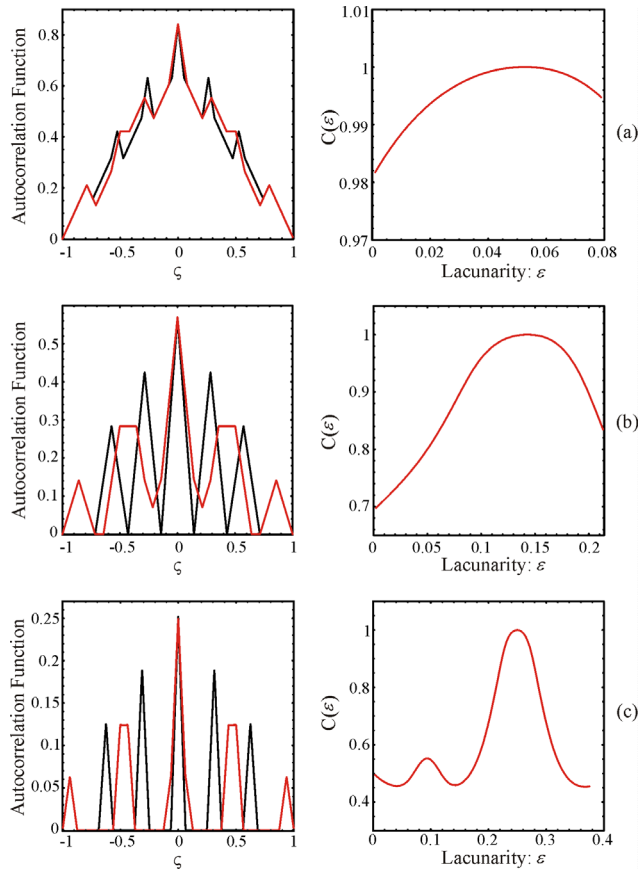


Fig. 5. Left: Autocorrelation function $q_\varepsilon(\xi) \otimes q_\varepsilon(\xi)$ for the FZPs shown in Fig 2, for $\varepsilon = \varepsilon_R$ (black) and for $\varepsilon = \varepsilon_{max}$ (red). Right: $C(\varepsilon)$ for the same FZPs. The animations Fig. 5(a).gif (311kB), Fig. 5(b).gif (498kB) and Fig. 5(c).gif (519kB), show the evolution of these functions for a variable ε .

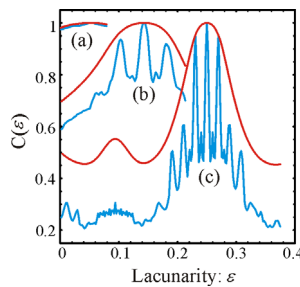


Fig. 6. $C(\varepsilon)$ for the pupils shown in Fig. 2 (red) and the corresponding ones with $S=2$ (blue).

5 Conclusions

FZPs with variable lacunarity has been extensively analyzed. The construction restrictions and the interrelations between the different parameters have been investigated. As a result, it was shown that the lacunarity has a dramatic effect on the axial irradiance provided by different FZPs with the same fractal dimension, but the essential aspects of the self-similarity are

preserved. A new parameter that correlates the axial irradiances given by FZPs with different lacunarity was proposed and its fractal behavior was reported.

The present study brings new lights on the powerful potential applications of FZPs, especially in scientific and technological areas where conventional zone plates have been successfully applied. Particularly, recent proposals of optical tweezers use phase filters to facilitate the trapping of particles in three-dimensional structures [14], spatial light modulators can be employed to display tunable FZPs producing focal spots that could be useful for this purposes. On the other hand, the non-uniform distribution of FZPs focal points along the optical axis could be exploited in the design of multifocal contact lenses for the correction of presbyopia. In this case a mechanism to control the diffraction efficiency of the FZP should be first developed. Currently we are investigating several properties of non-binary FZPs like the influence of optical aberrations, and polychromatic illumination. In particular, the attributes of rotationally non-symmetric FZPs, as elliptical or vortex FZPs, will be published in a forthcoming paper.

Acknowledgments

This research has been supported by the following grants: DPI 2003-04698 (Plan Nacional I+D+I Ministerio de Ciencia y Tecnología, Spain) and GV04B-186 (Generalitat Valenciana, Spain).